Metal Halide Perovskite-Based Heterojunction Photocatalysts

Haowei Huang,[a] Davy Verhaeghe,[a] Bo Weng,[a]* Biplab Ghosh,[a] Hongwen Zhang,[a] Johan Hofkens,[b] Julian A. Steele,[a] Maarten B. J. Roeffaers[a]*

[a] Dr. H. Huang, D. Verhaeghe, Dr. B. Weng, Dr. B. Ghosh, Dr. H. Zhang, Dr. J. A. Steele, Prof. M. B. J. Roeffaers

cMACS, Department of Microbial and Molecular Systems, KU Leuven, Celestijnenlaan 200F, 3001 Leuven, Belgium

E-mail: maarten.roeffaers@kuleuven.be; bo.weng@kuleuven.be

[b] Prof. J. Hofkens

Department of Chemistry, KU Leuven, Celestijnenlaan 200F, 3001 Heverlee, Belgium

Supporting information for this article is given via a link at the end of the document.

Abstract: With fascinating photophysical properties and strong potential to utilize solar energy, metal halide perovskites (MHPs) have become a prominent feature within photocatalysis research. However, the effectiveness of single MHP photocatalysts is relatively poor. The introduction of a second component to form a heterojunction represents a well-established route to accelerate carrier migration and boost reaction rates, thus increasing the photoactivity. Recently, there have been several scientific advances related to the design of MHP-based heterojunction photocatalysts, including Schottky, type-II, and Z-scheme heterojunctions. In this Review, we systematically discuss and critically appraise recent developments in MHP-based heterojunction photocatalysis. In addition, the techniques for identifying the type of active heterojunctions are evaluated and we conclude by briefly outlining the ongoing challenges and future directions for promising photocatalysts based on MHP heterojunctions.

1. Introduction

While metal halide perovskites (MHPs) have been known to researchers since the end of the 19th century,[1] they have received significant research interest in recent times, mainly due to their potential application as cheap and efficient solar cells.[2] In just over a decade, the power conversion efficiency of MHP-based solar cells has surged beyond 25%, making them the most efficient thin-film solar cells.[3] Given that many of the photophysical and optoelectronic properties required for efficient photovoltaics also coincide with the requirements for efficient photocatalysts, the applications of MHPs in photocatalysis have also garnered significant momentum recently.[4] MHPs are ionic crystals with a chemical formula of ABX_3 (Figure 1A), where A is a monovalent cation, being either organic (e.g., MA^+ ($H_3NH_3^+$) or FA^+ ($CH(NH_2)_2^+$) or inorganic (e.g. Cs^+), B is a divalent metal cation, such as Pb^{2+}, Sn^{2+}, and Ni^{2+}, which is coordinated with six halogen anions X (e.g. I^-, Br^- or Cl^-), forming a corner-shared $[BX_6]^{4-}$ octahedral network. However, the typical photocatalytic reaction conditions involving polar solvents, such as water, are not compatible with the MHPs due to degradation and even dissolution of the ionic structure. Recently, Roeffaers et al. have detailed the instability issues of MHP photocatalysts, whereby several proven strategies, including the use of saturated halo acid solutions and low-polarity solvents, as well as the MHP encapsulation and surface capping, for stabilizing MHP photocatalysts were outlined (Figure 1B).[4]

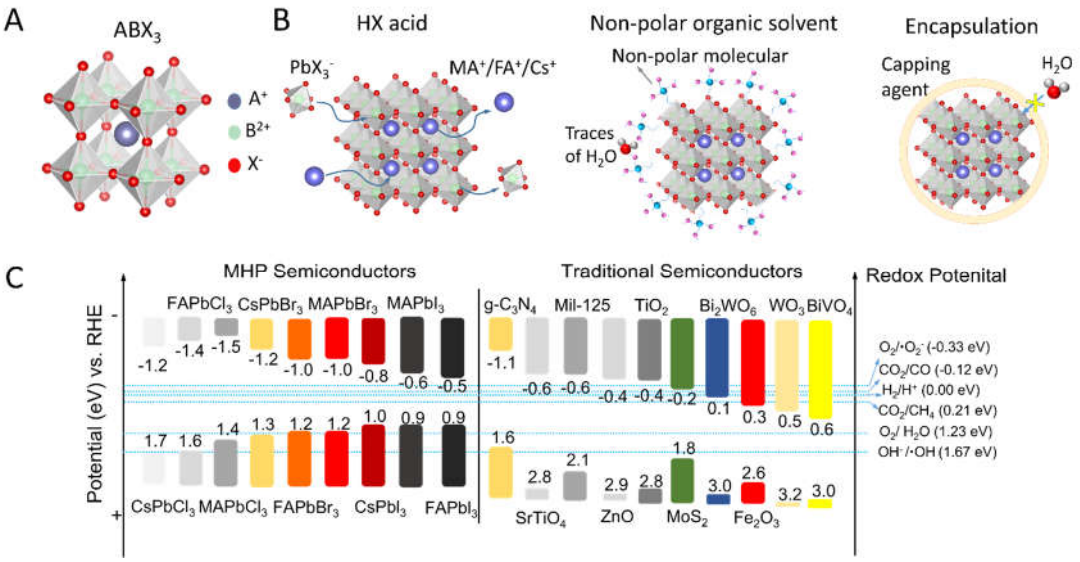

Figure 1. (A) the general crystal structure of MHPs; (B) Three main routes toward creating stable reaction environments when employing MHPs as a photocatalyst; (C) the valence band (VB) and conduction band (CB) positions of a selection of MHPs and traditional semiconductors relative to a selection of relevant redox reactions; all versus the reversible hydrogen electrode (RHE). Reproduced with permission from ref 4. Copyright 2020, American Chemical Society.

Beyond instability issues, a centrally important research goal is to understand and, ultimately, improve the photocatalytic performance. The photocatalytic activity is generally determined by three main factors: (i) the amount of light absorption and electron/hole pair formation; (ii) the efficiency of photogenerated charge carrier (electrons and holes) separation and migration; and (iii) the surface redox reaction rates.[5] The optical bandgap, the nature of the bandgap (direct or indirect), and the absorption coefficient define the amount of light that can be absorbed to generate charge carriers. As direct bandgap semiconductors, MHPs have a strong absorption coefficient, > 10^{-5} cm^{-1},[6] originating from the halide(*p*) orbitals to metal(*p*) orbitals transition at the band edge. Further, MHPs, as narrow bandgap semiconductors (Figure 1C),[7] have a broad absorption in the solar spectrum which can be further tuned by the substitution of different species at the *A*-, *B*- and *X*-sites.[8] For example, through exchanging the halides at the *X*-site, the absorption edge can be readily modified from blue (Cl-rich) to green (Br-rich) to red (I-rich).[8] MHPs also provide an excellent "environment" for photogenerated charge carrier generation and migration.[8,9] Having small exciton binding energy (for example E_b < k_bT in the triiodide family), free electron-hole pairs generation in MHPs are predominant when

optically excited.[8] Due to the small effective mass of electrons and holes in MHPs, for example in $MAPbI_3$ the electron and hole effective mass are about $0.1m_0$-$0.15m_0$ (m_0 is the free-electron mass), the carrier mobility in MHPs can reach up to ~10^2 cm^2 V^{-1} s^{-1} resulting in the easy separation and fast migration of the photogenerated electrons and holes.[10–12] At the same time, the charge carrier lifetimes in MHPs fall in the range of hundreds of nanosecond which ensure that the photoexcited carriers can travel easily through the material over hundreds of nanometer.[8] The highly polarizable crystal lattice and antibonding valence band further induce unique defect tolerant properties in MHPs, *i.e.*, easy-to-form intrinsic defects either lie near the band edges or within the bands and do not act as detrimental trap states during charge carrier migration.[13] As result, the probability of photoexcited carriers migrating to the MHP surface before recombination is high, thus leading to high efficiency of MHPs. For example, Xu *et al.* have recently reported that the photocatalytic activity is higher with $Cs_{2.3}MA_{0.7}Sb_2Br_9$ perovskite than that with classic photocatalysts (TiO_2, WO_3, and CdS). (Angew. Chem. Int. Ed. 2020, 59, 18136 – 18139). Apart from these excellent optoelectronic properties, the absolute band energies of MHPs are well-positioned with respect to various photocatalytic reactions to drive efficient photocatalytic activities. For example, many of the MHPs have a relatively negative conduction band minimum (CB) that meet the thermodynamic requirements to drive reduction reactions and produce superoxide radicals (Figure 1C). Notably, the oxidizing power of holes in MHPs is still limited since the valence band maximum (VB) of most MHPs is relatively high as compared with traditional photocatalysts. Actually, most of the MHPs cannot produce the free radicals with a high oxidative capacity (e.g., hydroxyl radicals) and this may hamper their photocatalytic applications to some extent.

Moreover, in the typical photocatalytic reactions, the surface redox reaction is in the millisecond timescale which is much slower than the charge carrier generation (in picosecond), migration (in pico/nanosecond), and even recombination (in nano/microsecond), leading to significant amounts of unwanted recombination.[14,15] Therefore, to further prolong the photoexcited carrier lifetime and facilitate the reactions at the surface, heterojunction photocatalysts are widely aimed to achieve higher photocatalytic efficiency. By combining the MHP-based photocatalyst to a second (semi)conductor, a heterojunction can be formed to enhance the spatially separation of photoexcited electrons and holes.[16] Besides boosting charge separation, the second material can also act as a cocatalyst to further improve

the surface reaction.[17] Therefore, the construction of an MHP-based heterojunction is an effective approach for improving the photocatalytic activity. Furthermore, compared with conventional semiconductors, the facile band structure engineering of MHPs is thus beneficial for heterojunction construction. Generally, the band-edges of MHPs are composed by hybridization between *B* and *X*'s orbitals,[8] which can be tuned by either substituting the halides or metal cations. For example, VB energies of MHPs follows the order $E^{Cl} < E^{Br} < E^{I}$, a trend following electronegativity of the halide anions. More importantly, the Fermi level of MHPs plays another determining role in the generation of the internal field upon heterojunction formation, which can be tuned by chemical doping, introducing halide vacancies (or removing them) or even defect-induced self-doping.[18–21]

In this review, we assesses the recent progress in engineering MHPs-based heterojunction photocatalysts including MHP-based type-II heterojunction, Z-scheme (direct and indirect), as well as MHP-non-semiconductor heterojunctions. We begin with the underlying photophysical principles of the different types of heterojunctions, the material requirements and examine their effectiveness in photocatalysis. In particular, we highlight several techniques deployed for the characterization of charge transfer in the heterojunction systems and we conclude by offering some perspective for the current challenges faced when looking to develop highly efficient MHP-based heterojunction photocatalysts moving forward

2. Impact of heterojunction formation on MHP-based photocatalysts

Figure 2 summarizes the most relevant heterojunctions that can be used to boost the photocatalytic performance of MHPs in combination with (1) a conducting material resulting in the formation of Schottky junction; (2) a complementary semiconductor material resulting in the formation of type-II and Z-scheme heterojunctions.

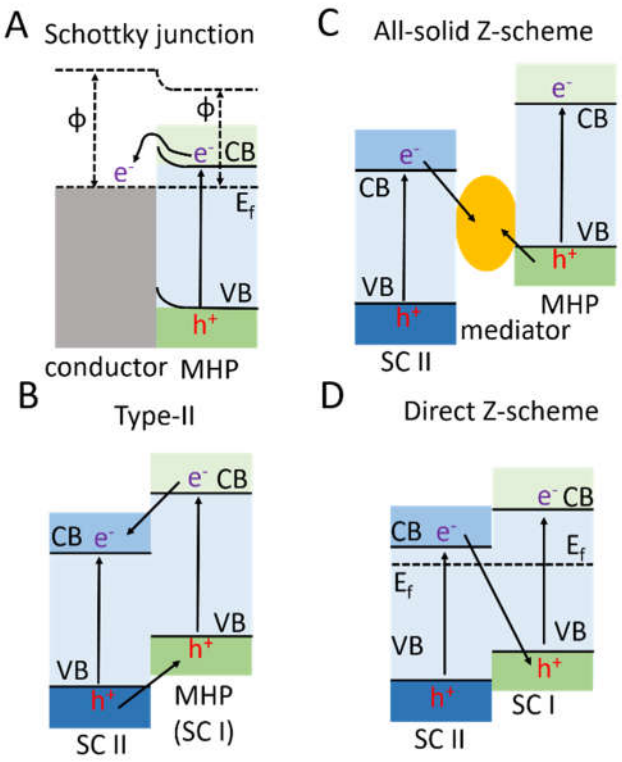

Figure 2. Schematic illustrations of various junctions between (A) conductor and MHPs (Schottky junction); as well as semiconductor-MHP heterojunction structures: (B) type-II, (C) all-solid Z-scheme, (D) direct Z-scheme. Φ: Work function; E_f: Fermi level; SC: Semiconductor; VB: Valence band; CB: Conduction band, e: electron; h: hole.

2.1 MHP-conductor heterojunction photocatalysts

Generally, the Fermi energy (E_f) of conductors, such as Pt, Au, Pd, and carbon materials, is located about ~0.5-1.0 eV vs RHE, which is relatively positive compared to that of MHPs (< 0.5 eV vs RHE).[15,22–27] After contact, an upward band bending at the MHP-conductor interface due to the band alignment results in the formation of a Schottky barrier (Figure 2A).[28–32] Note, band bending is a concept that is well described for bulk semiconductors,[33] the width over which bands bend generally takes several hundreds of nanometers and decreases with decreasing particle size. Thus, this concept has limited applicability to nanomaterials with radii in the range of tens of nanometers. The band bending schematically depicted in Figure 2 and described in this manuscript are thus a well-accepted simplification as it does gives an intuitive description of the changes in the electronic structure of materials after contact.[5] The charge conducting materials function here as both electron extracting

layer and cocatalysts, thus enhancing the photogenerated charge separation and surface reaction rate concomitantly.

The first report on MHP-based photocatalysis by Nam and coworker found that the addition of Pt nanoparticles on $MAPbI_3$ resulted in 1.8 times increased H_2 evolution.[34] In this work, the Pt modification not only formed a Schottky barrier thus enhancing the extraction of photogenerated electrons from $MAPbI_3$ but also acted as the cocatalyst accelerating the H_2 production. Following this example, Pt nanoparticles have been widely employed for enhancing the photocatalytic performance of MHPs, such as $CsPbBr_{3-x}I_x$,[35] $MAPbBr_{3-x}I_x$,[36] and $MA_3Bi_2I_9$[37]. Recently, H_2 evolution rates of 6.826 mmol g^{-1} h^{-1} under 1-sun illumination was achieved with $FAPbBr_{3-x}I_x$ decorated with Pt single atoms which corresponds to a solar-to-hydrogen conversion of 4.5%.[38]. Beyond Pt, other metals like Pd and Au nanoparticles have also been reported to promote the catalytic efficiency of MHPs.[28,29,30] However, the scarcity and high cost of these noble metals potentially limit their large scale usage. Carbon materials, such as carbon nanotubes, graphene and reduced graphene oxide (rGO) are low-cost alternatives that also offer excellent electron mobility and are potential candidates to construct Schottky junctions with MHPs. For example, Huang et al. hybridized rGO to $MAPbI_3$ and found a 67-fold enhanced photocatalytic H_2 evolution under visible light irradiation ($\lambda \geq 420$ nm).[42]

2.2 MHP-based type-II heterojunction photocatalysts

Three types of band alignment can occur when two semiconductors come in contact: the straddling gap (type-I), the staggered gap (type-II) and the broken gap (type-III) alignment.[16]. Type-I and type-III band alignments are not preferable for photocatalysis due to the inherent 50% charge carrier recombination (and hence loss) in combination with the loss in redox power in type-I and the absence of direct synergistic effects in type-III. In type-II heterojunctions, the CB and VB positions of semiconductor II (SC II) are lower than the corresponding bands of SC I leading to partly overlapping bandgaps (Figure 2B). Due to the relatively negative CB and positive VB of MHPs as compared to other potential semiconductors (Figure 1C), the MHPs usually act as SC I in the type-II heterojunctions. In this scenario, the photogenerated electrons in MHP (SC I) will migrate and accumulate on SC II while the holes from SC II transfer to the MHP. Note that p-n junction can be considered as a special type-II junction, which creates a strong internal electric field (IEF) at the interface to accelerate the

electrons and holes separation in opposite direction, leading to a more efficient and rapid charge separation compared to a normal type-II junction.[5] There is only one report to claim p-n junction formation with an MHP ($MASnI_3/TiO_2$), but without evidence.[43]

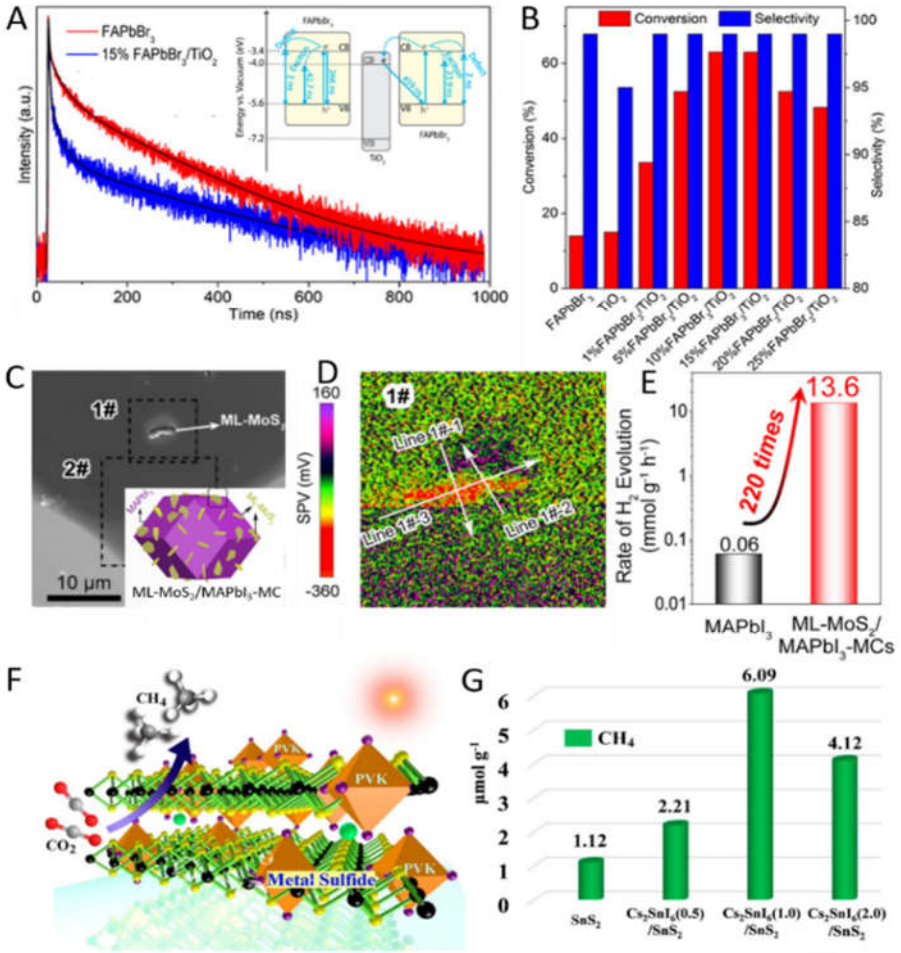

Figure 3. (A) Photoluminescence (PL) decay spectra of $FAPbBr_3$ and 15% $FAPbBr_3/TiO_2$ with the corresponding photoinduced charge transfer shown in inset and (B) photocatalytic oxidation of benzyl alcohol over pure $FAPbBr_3$, TiO_2, and a series of $FAPbBr_3/TiO_2$; Reproduced with permission from ref 44. Copyright 2018, American Chemical Society. (C) SEM and structural configuration of ML-MoS_2/$MAPbI_3$-MCs, (D) SPV image of the Region 1# in SEM, and (E) H_2 releasing rate over pure $MAPbI_3$ and ML-MoS_2/$MAPbI_3$-MCs; Reproduced with permission from ref 45. Copyright 2020, Elsevier. (F) schematic illustration and (G) activity of the photocatalytic CO_2 reduction over Cs_2SnI_6/SnS_2. Reproduced with permission from ref 46. Copyright 2019, American Chemical Society.

Roeffaers and coworkers reported the first MHP-based type-II heterojunction, using $FAPbBr_3/TiO_2$,

for selective photocatalytic oxidation of benzylic alcohols (BA) under simulated solar illumination.[44] Using time-resolved PL (Figure 3A), it was shown that the lifetime of the photoexcited charge carriers drastically increases from 266 ns to 459 ns, resulting in a 4-fold enhanced performance (Figure 3B). A similar MHP-based type-II heterojunction can also be used for solar fuel generation. Zhao and coworkers prepared $MAPbI_3$ microcrystal ($MAPbI_3$-MC)/monolayer MoS_2 nanosheets (ML-MoS_2) photocatalysts.[45] To verify the formation of type-II heterojunction, Kelvin probe force microscopy (KPFM) was used to measure the surface photovoltage (SPV) under light irradiation. The authors observed positive and negative SPV of MoS_2 and $MAPbI_3$, respectively, which is caused by the accumulation of photogenerated electrons and holes (Figure 3C and D). However, these values do not provide sufficient evidence of the charge carrier migration between the SCs in the composite. Comparative SPV measurement in presence and absence of light irradiation would yield a more detailed insight. The measured H_2 evolution rate (13.6 ± 1.2 mmol g^{-1} h^{-1}) over the composite ML-MoS_2/$MAPbI_3$-MCs in a saturated aqueous HI/H_3PO_2 solution under visible light irradiation, is 220 times higher than that of the pure $MAPbI_3$-MCs (Figure 3E) and an impressive solar-to-hydrogen conversion efficiency of 1.18% was achieved. The efficiency of charge migration between two materials forming a heterojunction can be further improved by strengthening the interfacial contact. Recently, Kuang et al. showed that Cs_2SnI_6 nanocrystals formed an intimate contact with SnS_2 nanosheets due to the shared Sn atoms at the interface (Figure 3F).[46] The S···Sn···I bonds were formed between Cs_2SnI_6 and SnS_2, which can act as direct charge transfer channels to effectively facilitate the charge carrier transfer. After optimization, the CH_4 formation rate of Cs_2SnI_6/SnS_2 composites was 5.4 times higher than that of pristine SnS_2 (Figure 3G).

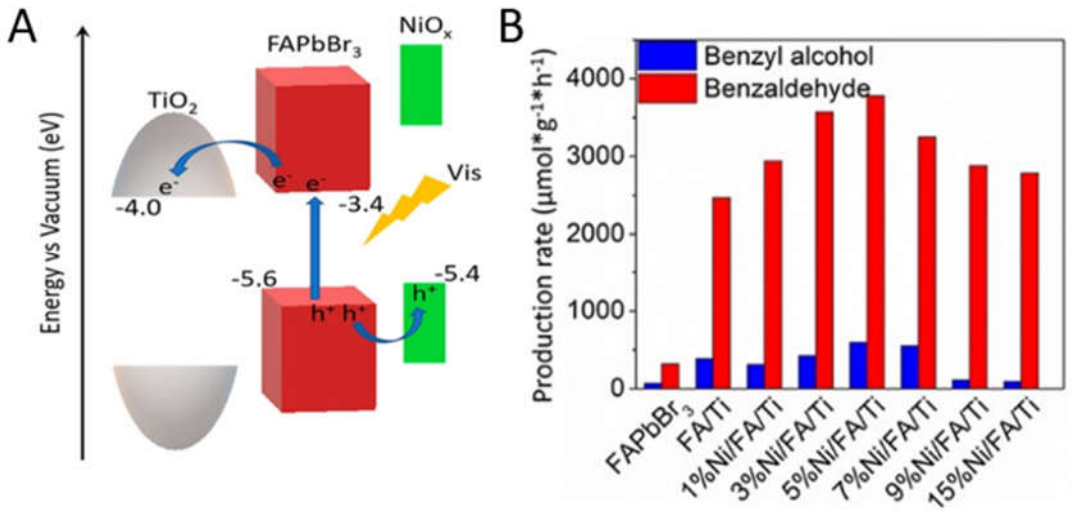

Figure 4. (A) Schematic of the carrier transfer over the $NiO_x/FAPbBr_3/TiO_2$; (B) Photocatalytic oxidation of $C(sp_3)$–H over pure $FAPbBr_3$, $FAPbBr_3/TiO_2$, and a series of $NiO_x/FAPbBr_3/TiO_2$ (Ni/FA/Ti) hybrids. Reproduced with permission from ref 47. Copyright 2019, American Chemical Society.

Beyond binary composites, multi-component MHP-based photocatalysts have also been reported to further improve the charge carrier transfer and photocatalytic performance. One example is the addition of a hole extracting layer (NiOx) to a type-II $FAPbBr_3/TiO_2$ heterojunction (Figure 4A).[47] The improved charge separation, as proven by time-resolved PL, resulted in a 12-fold increase in photocatalytic selective oxidation of $C(sp^3)$–H (Figure 4B). Similar results were reported by Li et al. when modifying $MAPbBr_3$ with poly(3,4-ethylenedioxythiophene) polystyrenesulfonate (PEDOT:PSS) and Pt/Ta_2O_5 as hole- and electron- transporting materials, respectively, leading to an impressive 52-fold improved H_2 evolution.[48] However, it is worth noting that unlike layer by layer structure in solar cells, these three-component photocatalysts are heterogeneous. It can be expected that interfaces form between NiO_x and TiO_2 or PEDOT:PSS and Pt/Ta_2O_5 which gives an alternative recombination path for electrons and holes at these interfaces. In reality, the interfaces formed in these more complex multi-component materials and the carrier transformation and recombination are more complex than the simplified schematic picture shown in Figure 4A. To avoid this issue, Roeffaers et al mimicked MHP solar cells to develop a layer-by-layer $NiO_x/CsPbB_{r3}/TiO_2$ planar heterojunction photocatalyst for boosting the photocatalytic performance.[49]

In recent years, various MHP-based type-II heterojunctions have been prepared and used in a wide range of chemical reactions, including water splitting, CO_2 reduction reaction, organic transformation, and environmental remediation (Table S1). The construction of MHP-based type-II heterojunctions can not only enhance the photocatalytic performance but also improve the stability of MHPs. For instance, a $NiO_x/CsPbB_{r3}/TiO_2$ planar heterojunction photocatalyst was designed, among which the TiO_2 and NiO_x layers can not only extract photogenerated electrons and holes, respectively, but also serve as protecting layers to improve the stability of $CsPbBr_3$. The photocatalytic BA oxidation activity over $NiO_x/CsPbBr_3/TiO_2$ heterojunction is 7 times higher than that of $CsPbBr_3$ counterpart and a long term photostability (over 90 h) is demonstrated. Additionally, Kamat et al. reported a quasi-type II $CsPbBr_3$-CdS heterojunction and the deposition of CdS could provide solvent stability in toluene/ethanol mixed solvent, resulting improved stability and photocatalytic performance over $CsPbBr_3$–CdS heterostructure as compared with $CsPbBr_3$. (Chemical Science 2021, 12, 14815-14825) Similar polar solvent stability enhancement was also observed by Nag and coworkers, who found that the luminescence of core/shell (pseudo type-II) $CsPbBr_3$/ZnS nanocrystals can retain after being dipped in water for more than 2 days.(*ACS Energy Lett.* 2020, 5, 6, 1794–1796) However, MHP-based type-II heterojunctions also have their limitations. For instance, the injection of electrons from the CB of MHPs to the CB of SC II will reduce the overall reduction ability, and the holes moving from the VB of SC II to the VB of MHPs results in a loss of oxidative power (Figure 2B). Moreover, if the catalytic reactions are kinetically not matched to the photocarrier generation, this will lead to the accumulation of charges that impede the further separation. Due to lattice mismatch or poor contact between the two components, the interface may also serve as additional source of charge trapping or recombination centers for the charge carriers. Therefore, despite the exploitation of the advantageous charge transfer in MHP-based type-II heterojunctions, these disadvantages must also be taken into consideration for achieving high photocatalytic efficiency.

2.3 MHP-based Z-scheme heterojunction photocatalysts

The difference between Z-scheme and type-II heterojunctions is the direction of photogenerated charge carrier migration (Figure 2C and D). Specifically, electrons in the CB of SC II migrate to the VB of SC I and recombine with the holes, while the electrons in the CB of SC I and holes in the VB of SC II are preserved. As a result, Z-scheme heterojunctions possess a strong redox ability. Considering the

strong reduction power of the electrons and weak oxidation power of the holes generated in MHPs (Figure 1C), MHPs are most likely to act as SC I in the Z-scheme heterojunctions. However, in Z-scheme heterojunctions, 50% of the charge carriers recombine at the interface, thus lowering the solar energy conversion efficiency since two photons, rather than one, are required to create a catalytically active electron-hole pair. There are three types of Z-scheme heterojunction, traditional Z-scheme heterojunction, all-solid-state Z-scheme heterojunction, and direct Z-scheme heterojunction.[50] In traditional Z-scheme heterojunctions, the electrons from the CB of SC II are transported to the VB of SC I via a redox couple like I^-/IO_3^-,[51] but this has so far not been reported among MHP-based photocatalysts. The all-solid-state Z-scheme heterojunction is composed of two semiconductors combined through a charge conductor, such as a metal or carbon material, that acts as the electron mediator (Figure 2C). On the other hand, direct Z-scheme heterojunction consists of two semiconductors in direct contact. Direct Z-scheme systems do not rely on an electron mediator but make direct contact and an internal electric field directs the charge migration.

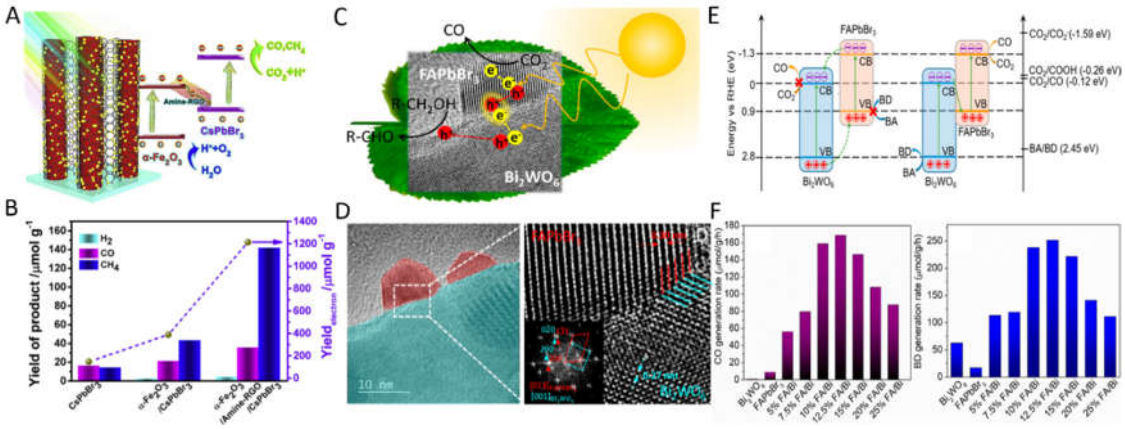

Figure 5. (A) Schematic illustration of an all-solid-state Z-scheme photocatalyst: Fe_2O_3/RGO/$CsPbBr_3$ and (B) the photocatalytic performance in the CO_2 reduction; Reproduced with permission from ref 53. Copyright 2020, Elsevier. (C) Schematic illustration of a direct Z-Scheme $FAPbBr_3/Bi_2WO_6$ photocatalyst; (D) HRTEM of $FAPbBr_3/Bi_2WO_6$ revealing the semi-coherent interface; (D) Energy diagram, charge dynamics on of $FAPbBr_3/Bi_2WO_6$; (F) CO and BD generation rate over pure Bi_2WO_6, $FAPbBr_3$, and a series of $FAPbB_{r3}/Bi_2WO_6$ PC with different relative amounts. Reproduced with permission from ref 15. Copyright 2020, American Chemical Society. VB: Valence band; CB: Conduction band; BD: benzaldehyde; BA: benzyl alcohol.

In the past decade several Z-scheme photocatalysts have been reported, the first report on MHP-based Z-scheme photocatalysts was only published in 2020 by Kuang *et al*.[52] This all-solid-state Z-scheme was based on $CsPbBr_3$ (SC I) coupled to α-Fe_2O_3 (SC II) using amine-functionalized reduced graphene oxide (RGO) as electron mediator (Figure 5A). The reported Z-scheme photocatalyst had a 6-fold increase in photocatalytic activity for the CO_2 to solar fuels (CO and CH_4) reduction (12.1 μmol g^{-1} h^{-1}) (Figure 5B). However, the chosen reaction could equally well be driven by an MHP-based type-II heterojunction thus not maximally exploiting the added value of this type of heterojunction.[53] Furthermore, all-solid-state Z-scheme heterojunctions suffer from light shielding by the electron mediator.

Roeffaers *et al* reported a direct Z-scheme heterojunction of $FAPbBr_3/Bi_2WO_6$ with a semicoherent interface[15] (Figure 5C and D). To fully exploit the strong redox ability of the Z-scheme system, BA instead of water was selectively oxidized by the photogenerated holes to generate benzaldehyde (BD) (Figure 5E). The direct Z-scheme charge transfer between the SCs was confirmed with transient mid-infrared (mid-IR) absorption (details will be discussed in the next section). Under simulated solar irradiation, a CO evolution rate of 170 μmol g^{-1} h^{-1}, which is the highest CO release rate over MHP photocatalysts to date, was coupled to 250 μmol g^{-1} h^{-1} BD production (Figure 5F). One of the main assumptions in this work was that a good interfacial contact causes a better interfacial charge transfer resulting in a better activity.

Table S2 summarizes the reports on MHP based Z-scheme photocatalysts. In most reports CO_2 reduction is coupled to H_2O oxidation, reactions that do not utilize the high redox power of the Z-scheme heterojunction and that could be performed by the common type-II heterojunctions. Due to the good redox power of the photogenerated electrons and holes, there is lots of potential for these systems to be used in more challenging reactions that require larger redox power. On the other hand, current reports reveal that different types of heterojunctions have been proposed to form for the same material combinations. For example, Tüysüz et al. prepared a type-II heterojunction $CsPbBr_3/TiO_2$ photocatalyst,[54] while Yu and coworkers prepared a Z-scheme photocatalyst with the same two components $CsPbBr_3$ and TiO_2.[55] For $FAPbBr_3/Bi_2WO_6$ it was shown that part of the electrons will follow the Z-scheme pathway and the others move as type-II heterojunction, indicating that the direct Z-scheme and type-II heterojunction may coexist under certain conditions. The latter is not surprising

if one takes the heterogeneity present in most materials into consideration. Moreover, the coexistence of Type-II and Z-scheme should also present in other semiconductor-semiconductor heterojunctions (e.g., g-C_3N_4/TiO_2)(10.1016/j.apsusc.2016.06.145; Langmuir 2020, 36, 21, 5967–5978) and CdS/TiO_2,(ACS Omega 2021, 6, 28, 18178–18189; https://doi.org/10.1016/j.apsusc.2017.06.028) while direct evidence to demonstrate this charge transfer process is still lacking.

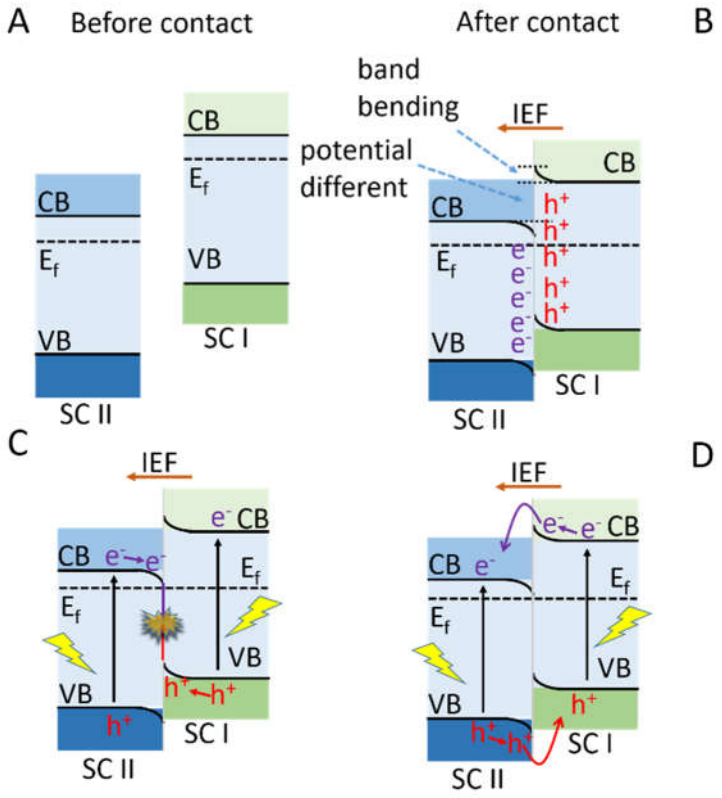

Figure 6. The relative band positions and Fermi level of SC I and SC II (A) before and (B)after contact. With the light irradiation, the charge migration fellows the Z-scheme (C) and type-II (D). E_f: Fermi level; SC: Semiconductor; VB: Valence band; CB: Conduction band; IEF: internal electric field.

Fundamentally, the relative band positions of SC I and SC II as well as their Fermi levels, are key features that define the development of the internal electric field (IEF) upon contact and hence the charge transfer direction. In a typical heterojunction, the CB, VB, and Fermi level of SC II are more negative than the corresponding ones in SC I (Figure 6A). After contact, an IEF and band bending will form at the interface between SC I and SC II because of the band alignment between SC II and SC I (Figure 6B). With light irradiation, the IEF drives the photogenerated electrons in SC II to the SC I and recombine with the photogenerated holes in SC I; this is the essential step defining Z-scheme

photocatalysis (Figure 6C). However, due to the potential difference of CBs and VBs in SC I and SC II, the electrons in SC I CB spontaneously move to a more positive SC II CB, while the holes move to a more negative SC I VB from SC II VB, to follow a type-II pathway. However, the energy barriers caused by band bending, which impede the type-II charge transfer, should also be taken into consideration (Figure 6D). In principle, regulating the Fermi levels e.g., through doping, is key for obtaining a larger band bending and internal electric field, leading to improved Z-scheme dynamics, and reducing the potential difference between the CBs and VBs of SC I and SC II. Additionally, due to the differences in the photon absorption and charge carrier generation efficiencies of two semiconductors, optimizing the ratio between SC I and SC II to balance the charge carrier generation in both semiconductors is also an important factor determining the overall efficiency of a Z-scheme photocatalyst. Since the band structure tuning, including CB, VB, and Fermi levels in MHPs is rather straightforward,[56] it is possible to construct highly efficient heterojunctions via band structure engineering in the future.

3. Photophysical characterization approaches for evaluating different types of active heterojunctions

As described above, the inherent heterogeneity of heterojunction materials can result in complex migration behavior of the photoexcited charge carriers; some charges follow type-II while others follow Z-scheme. It is hence important to confirm the primary pathways of photoexcited charge carrier migration and identify the nature of heterojunctions formed. Currently, several methods have been developed that can be used to provide insights into the nature of the created heterojunction such as (1) self-confirming photocatalytic reaction; (2) *in-situ* X-ray photoelectron spectrum (XPS); (3) *in-situ* KPFM; (4) transient absorption.

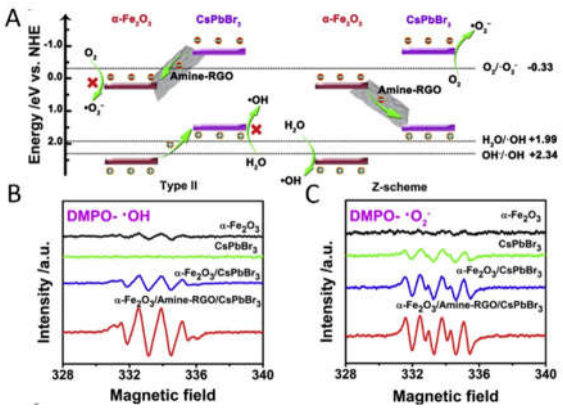

Figure 7. (A) Energy band diagram and reaction mechanism of type-II and Z-scheme heterojunctions of Fe_2O_3/RGO/$CsPbBr_3$; ESR spectra of DMPO-·OH (B) and DMPO-·O_2^-(C) in the presence of Fe_2O_3, $CsPbBr_3$, Fe_2O_3/$CsPbBr_3$, and Fe_2O_3/RGO/$CsPbBr_3$. Reproduced with permission from ref 52. Copyright 2020, Elsevier. DMPO: 5,5-Dimethyl-1-pyrroline N-oxide.

One of the most apparent differences between type-II and Z-scheme photocatalysts is the oxidizing and reducing ability of the holes and electrons. By selecting photocatalytic half-reactions, solely driven by Z-scheme heterojunctions, its formation can be confirmed. For example, Kuang et al. used reactive oxygen species (•O_2^- and •OH) generation as probe reactions to prove the Z-scheme in Fe_2O_3/RGO/$CsPbBr_3$.[52] This is possible because the photogenerated electrons in the CB of Fe_2O_3 cannot reduce the O_2 to •O_2^-, and the photogenerated holes in the $CsPbBr_3$ VB cannot oxidize the water to •OH. If a type-II junction forms or is the primary pathway, no or less reactive oxygen species will be generated (Figure 7A). In contrast, with the primary pathway of Z-scheme, the photogenerated electrons and holes will accumulate on the CB of $CsPbBr_3$ and VB of Fe_2O_3 and react with O_2 and water to generate •O_2^- and •OH, respectively (Figure 7A). As shown in Figure 7B and C, the signals of •O_2^- and •OH are higher than that in single components, which confirms that in the reported Fe_2O_3/RGO/$CsPbBr_3$ material, at least part of the photogenerated charges follow a Z-scheme mechanism. Besides reactive oxygen species generation, some other self-confirming photocatalytic reactions can be used to characterize the formation of Z-scheme, such as the photocatalytic H_2O and/or CO_2 reduction for justifying the strong reduction ability, and the photocatalytic water oxidation and pollutant degradation for the strong oxidation ability. Note, the appropriate reaction selection should follow the band positions of two semiconductors. More importantly, the formation of strongly oxidizing holes and reducing electrons can also be observed, even if the Z-scheme is the minority, and

the type-II is the majority in a heterojunction. Therefore, it is not only about the detection of specific species, a semiquantitative analysis between the heterojunction and single components is also necessary to determine the heterojunction formation. Besides EPR, fluorescence techniques in combination with redox-responsive fluorogenic dyes are convenient semiquantitative tools.[57,58]

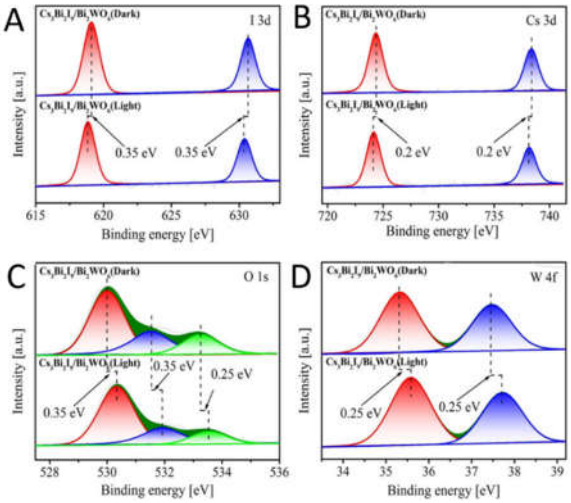

Figure 8. XPS of (A) I 3d, (B) Cs 3d, (C) O 1s and (D) W 4f with/without light irradiation. Reproduced with permission from ref 59. Copyright 2020, Wiley-VCH.

As the photoexcited charge carrier transfer between the two SCs under light irradiation changes the charge density at the surface, the electron binding energy of the elements can be probed directly by *in-situ* XPS. For instance, when a semiconductor gains electrons, its electron density increases leading to a measurable decrease in binding energy. Conversely, losing electrons increases the detected binding energy. Lu and coworkers developed a $Cs_3Bi_2I_9/Bi_2WO_6$ composite for CO_2 photoreduction, in which they used *in-situ* XPS to prove the Z-scheme charge transfer.[59] Specifically, under light irradiation, the electron binding energy of both I 3*d* and Cs 3*d* experiences negative shifts compared to those in dark (Figure 8A and B), while conversely, W 4*f* and O 1*s* exhibited slight shifts to higher energy (Figure 8C and D), indicating that the photogenerated electrons in Bi_2WO_6 migrate to $Cs_3Bi_2I_9$, following the Z-scheme. In practice, however, observations of only a minor shift in binding energy (i.e., in the range 0.1-0.2 eV) are commonly observed, and these are considered too close to the typical instrument and data processing errors. Therefore, relatively small shifts are suggested to act only as a supporting piece of evidence for the charge migration pathway, while more robust and conclusive support should be

aimed at.

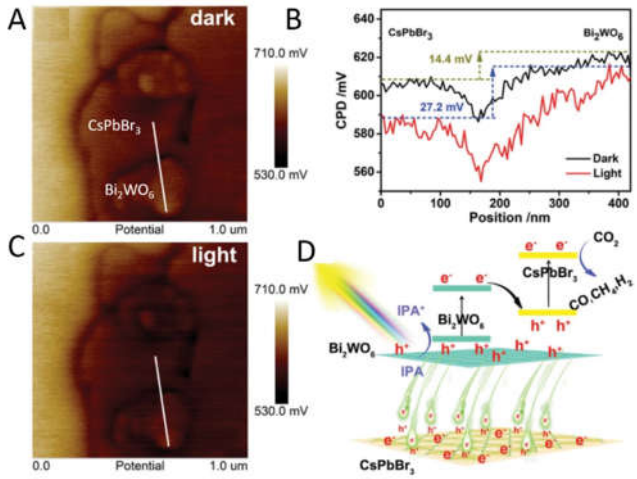

Figure 9. Surface potential images in the dark(A), under light(C) and the corresponding line profiles of surface potential(B); (D) Schematic diagram of the electron transfer on $CsPbBr_3/Bi_2WO_6$ Z-scheme heterojunction. Reproduced with permission from ref 60. Copyright 2020, Wiley-VCH. IPA: Isopropanol.

As a vivid example, the charge migration in the heterojunction formed by 2D materials can be detected by KPFM, which is a scanning probe technique for mapping the surface morphology and electric potential of 2D materials at the nanoscale. Scanning the interface between these 2D materials with/without light irradiation, the changes in surface potential can be used to identify the nature of carrier migration. In 2020, Kuang et al. prepared a 2D/2D heterojunction with $CsPbBr_3$ and Bi_2WO_6 for CO_2 reduction.[60] In the dark, the surface potential gap between $CsPbBr_3$ and Bi_2WO_6 is *ca.* 14.4 mV with $CsPbBr_3$ is lower than Bi_2WO_6 (Figure 9A and B). With UV light irradiation to excite both of them, this gap increases to 27.2 mV because the electrons and holes follow the Z-scheme pathway and accumulate on the $CsPbBr_3$ and Bi_2WO_6, respectively (Figure 9B-D). Currently, this technique still suffers several limitations. For instance, it is mostly suitable for 2D heterojunctions with an obvious surface potential gap and the identification of two components in the composite needs be assisted by additional techniques.

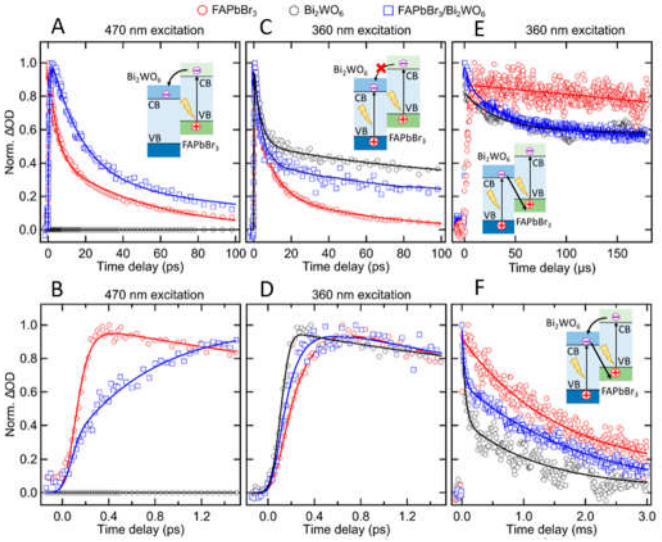

Figure 10. Time-resolved IR transient absorption traces from the Bi_2WO_6, $FAPbBr_3$, and $FAPbBr_3/Bi_2WO_6$. (A) Decay and (B) rising phase signals upon 470 nm excitation. (C) Decay and (D) rising phase signals upon 360 nm excitation. Decay phase signals upon 360 nm excitation over (E) microseconds and (F) milliseconds. The insets in A, C, E, and F depict electronic interactions derived from their respective transients. Reproduced with permission from ref 15. Copyright 2020, American Chemical Society.

Transient absorption (TA) spectroscopy is a powerful tool to comprehensively reveal the behavior of photoexcited carriers in a semiconductor. The transient changes in the material absorption, after above band gap excitation, contains information about the charge generation, transfer, and recombination. For example transient changes in the mid-IR absorption revealed the photogenerated charge transfer pathways in $FAPbBr_3/Bi_2WO_6$ photocatalyst.[15] Two pump light sources, 360 nm and 470 nm, were employed to illuminate the composite material and the pristine $FAPbBr_3$ respectively. With 470 nm pump light, an electron injection process from $FAPbBr_3$ to Bi_2WO_6 can be observed in the $FAPbBr_3/Bi_2WO_6$ in ps timescale like type-II heterojunction. (Figure 10A and B). Conversely, simultaneously pumping both components in the heterojunction with 360 nm irradiation, no electrons were injected from the CB of $FAPbBr_3$ to the CB of Bi_2WO_6 in ps timescale (Figure 10C and D). To reveal the recombination processes in the $FAPbBr_3/Bi_2WO_6$, the electrons kinetic trace in μs-ms timescale was analyzed. Compared to the pristine Bi_2WO_6 and $FAPbBr_3$ systems, an additional fast recombination process can be observed in the $FAPbBr_3/Bi_2WO_6$ which can be ascribed to the

recombination of electrons in the CB of Bi_2WO_6 with the VB holes in $FAPbBr_3$, namely, Z-scheme recombination process (Figure 10E). Note, in ms timescale the slow species in the $FAPbBr_3/Bi_2WO_6$ were longer than that in Bi_2WO_6 and $FAPbBr_3$ indicating that some electrons will follow the type-II pathway (Figure 10F). Based on transient absorption spectroscopy in combination with wavelength selective illumination, the details of photogenerated charge carrier behavior and the types of heterojunctions can be deduced, which in this case is a mix of type-II and Z-scheme. In such transient studies, the selection of the optical excitation sources, the observed absorption band and the timescale should be adapted to the material at hand. Specifically, to reveal the presence of Z-scheme charge migration, both components should be excited. The mid-IR is well suited to study electron migration, while with UV-Vis-NIR transient absorption, more detailed charge carrier dynamics information can be obtained.

Based on the aforementioned discussion, it is clear that a careful validation of the charge transfer pathway in heterojunction MHP photocatalysts is crucial. However, there are still some issues that need to be overcome. Specifically, when we employ (1) self-confirming photocatalytic reactions, (2) in situ XPS and (3) in situ KPFM to prove the Z-scheme or type-II, we can only confirm the primary pathway in the heterojunction rather than totally exclude the presence of the second pathway since the coexistence of Z-scheme and type-II heterojunction could also lead to the same results. Alternatively, TA spectroscopy is demonstrated to comprehensively monitor the behavior of photoexcited carriers in the composite catalyst and is believed to be a better choice to characterize the formed heterojunctions, which can not only reveal whether the coexistence of Z-scheme and type-II or not, but also quantitatively analyze the ratio of Z-scheme and type-II.

4. Summary and outlook

In the past decade, MHPs have been intensely explored and developed for a variety of optoelectronic applications. With their exceptional optoelectronic properties, MHP-based photocatalysis can also offer one of the most direct methods to utilize and store solar energy and thus has attracted significant attention recently. However, the performance of single component MHP photocatalysts is currently not effectively exploiting its full potential. To further improve the activity of MHP photocatalysts, various types of heterojunctions have been constructed. In this review, we provide an overview of the recent

progress in the field of MHP-based heterojunction photocatalysts and the important material properties that need to be taken into consideration for future research. Due to the difficulty of identifying the exact types of active heterojunctions involved, several techniques for probing the photogenerated charge carrier migration pathways have been detailed also. Based on our assessment of recent (proven) progress in the field of MHP-based heterojunctions, future research should be focused on the following aspects:

1. Type-II heterojunctions that maximize the utilization of the photogenerated charge carriers, however, at the cost of losing some of the potential driving force. Z-scheme heterojunctions on the other hand maximize the driving force of the photogenerated electrons and holes for chemical reactions however at the consequence of wasting half of the photogenerated charge carriers. Therefore, the target reactions and the required redox potentials (Figure 1) should take into consideration when designing and constructing of MHP-based heterojunction photocatalyst. For instance, some researchers have constructed $CsPbBr_3$ based Z-scheme for reducing CO_2 with water as electron source. Since the band positions of large bandgap $APbX_3$, with X = Br, Cl, meet the requirement of direct CO_2 reduction and water oxidation, type-II heterojunctions ultimately could be more efficient for this reaction. The development of Z-scheme $APbX_3$ photocatalysts should focus on reactions optimally benefiting a large driving force.[61] For example, small bandgap ABI_3 could be considered for extending the absorption spectrum and optimizing the solar light use, given that an appropriate stabilization can be found.[34] Additionally, by doping with halide and reducing halide vacancies, the Fermi level of MHPs in the heterojunction can be well tuned, by which the junction types will change from type-II to Z-scheme or vice versa, thus allowing better optimalization of heterojunctions for specific reactions with high photocatalytic performance.

2. Significant challenges still remain in controlling the structure, morphology, assembly, and engineering of the interface of MHP-based heterojunctions. Specifically, the crystal facets play a crucial role in determining the overall photocatalytic efficiency.[62] Therefore, the controlled synthesis of MHPs with well-defined crystal facets together with thorough theoretical support to achieve a deeper understanding of facet-dependent surface chemistry and the influence on carrier migration in a heterojunction is necessary. On the other hand, defects and grain

boundaries in MHPs can have multiple intertwined roles in light absorption, charge transport and recombination, often in opposing and counter-intuitive fashion. Thus, the role of defects whether they are in bulk or at the surface, need to be studied systematically to enable rational design of the MHP-based heterojunctions to maximize the photocatalytic activity.

3. The introduction of an external field can be used to further boost the charge carrier migration in MHP-based heterojunctions. In photoelectrocatalysis (PEC), the applied external electric field promotes charge separation, and increases redox reaction rates, thus improving the overall solar-to-fuel conversion efficiency. Besides electric fields, other external triggers, including mechanical stress, microwaves, magnetic field, and/or coupled fields, could improve the catalytic performance of MHPs from the inside out. For example, with external mechanical force, a built-in electric field will be created in the $MAPbI_3$ to effectively separate the photogenerated charge carriers, thus enhancing the final photoactivity.[63]

4. The poor interface and lattice mismatch in most heterojunctions leads to the formation of defect sites that might serve as charge trap sites and recombination centers, limiting the photocatalytic performance. Preparing an MHP homojunction can minimize the loss of photogenerated charge carriers at the interface. Further, by doping different halide ions to construct MHP-based multi-homojunctions with a funnel-shaped energy band structure,[64] the solar energy conversion efficiency can be promoted by simultaneously enhancing light absorption and charge separation through the generation of an extended band bending and an oriented electric field.

5. Lastly, the field would greatly benefit from the development of robust and easy-to-perform experimental methods that allow to study the fate of the photogenerated charges and identify the active heterojunction type. As explained above, the reported methods, like self-confirmed photocatalytic reaction, in situ XPS and in situ KPFM, can provide insights but do not allow to yield a very detailed picture on the fate of the photogenerated charge carriers. To date, TA spectroscopy in combination with selected wavelength PC photoactivation yields the most detailed picture, offering a more reliable and comprehensive understanding of the carrier pathway behaviors in the MHP-based composites. Moreover, even with the coexistence of Z-scheme and type-II, with TA it is possible to determine the relative contribution of both

heterojunctions to the overall process.

In the field of MHP-based photocatalysis, the fascinating properties of MHPs are not yet fully unleashed. In terms of efficient solar energy utilization, MHP-based heterojunction photocatalysts lags behind the MHP PV state of the art. Building on the rapid development of the latter, it can be expected that in the future MHP-based heterojunction photocatalysts will be continually developed using insights from MHP PV research and will achieve some breakthroughs in solar energy utilization, including both efficiency (> 10 % solar-to-fuels efficiency) and stability (thousands of hours). This review aims to give direction and stimulate further exploration of the MHP-based heterojunction systems in photocatalysis.

Acknowledgements

This work was financially supported by the Research Foundation – Flanders (FWO grant nos. G.0B39.15, G.0B49.15, G098319N, 1280021N, 12Y7221N, 12Y6418N, 1242922N, VS052320N and ZW15_09-GOH6316N), the KU Leuven Research Fund (C14/19/079, iBOF-21-085 PERSIST), KU Leuven Industrial Research Fund (C3/19/046), the Flemish government through long term structural funding Methusalem (CASAS2, Meth/15/04), the European Union's Horizon 2020 research and innovation programme under the Marie Skłodowska-Curie grant agreement No. 891276.

Keywords: Metal Halide Perovskite • Type-II • Z-Scheme• Heterojunction • Photocatalyst

References

[1] H. L. Wells, *Zeitschrift für Anorg. Chemie* **1893**, *3*, 195–210.

[2] M. A. Green, A. Ho-Baillie, H. J. Snaith, *Nat. Photonics* **2014**, *8*, 506–514.

[3] Best Research-Cell Efficiency Chart, https://www.nrel.gov/pv/assets/pdfs/best-research-cell-efficiencies-rev211011.pdf

[4] H. Huang, B. Pradhan, J. Hofkens, M. B. J. Roeffaers, J. A. Steele, *ACS Energy Lett.* **2020**, *5*, 1107–1123.

[5] H. Wang, L. Zhang, Z. Chen, J. Hu, S. Li, Z. Wang, J. Liu, X. Wang, *Chem. Soc. Rev.* **2014**, *43*, 5234–5244.

[6] F. P. García de Arquer, A. Armin, P. Meredith, E. H. Sargent, *Nat. Rev. Mater.* **2017**, *2*, 16100.

[7] A. K. Jena, A. Kulkarni, T. Miyasaka, *Chem. Rev.* **2019**, *119*, 3036–3103.

[8] J. S. Manser, J. A. Christians, P. V Kamat, *Chem. Rev.* **2016**, *116*, 12956–13008.

[9] L. M. Herz, *ACS Energy Lett.* **2017**, *2*, 1539–1548.

[10] L.-J. Wu, Y.-Q. Zhao, C.-W. Chen, L.-Z. Wang, B. Liu, M.-Q. Cai, *Chinese Phys. B* **2016**, *25*, 107202.

[11] M. Grätzel, *Nat. Mater.* **2014**, *13*, 838–842.

[12] C. C. Stoumpos, C. D. Malliakas, M. G. Kanatzidis, *Inorg. Chem.* **2013**, *52*, 9019–9038.

[13] H. Jin, E. Debroye, M. Keshavarz, I. G. Scheblykin, M. B. J. Roeffaers, J. Hofkens, J. A. Steele, *Mater. Horiz.* **2020**, *7*, 397–410.

[14] K. Takanabe, *ACS Catal.* **2017**, *7*, 8006–8022.

[15] H. Huang, J. Zhao, Y. Du, C. Zhou, M. Zhang, Z. Wang, Y. Weng, J. Long, J. Hofkens, J. A. Steele, M. B. J. Roeffaers, *ACS Nano* **2020**, *14*, 16689–16697.

[16] J. Low, J. Yu, M. Jaroniec, S. Wageh, A. A. Al-Ghamdi, *Adv. Mater.* **2017**, *29*, 1601694.

[17] J. Yang, D. Wang, H. Han, C. Li, *Acc. Chem. Res.* **2013**, *46*, 1900–1909.

[18] O. A. Lozhkina, A. A. Murashkina, V. V Shilovskikh, Y. V Kapitonov, V. K. Ryabchuk, A. V Emeline, T. Miyasaka, *J. Phys. Chem. Lett.* **2018**, *9*, 5408–5411.

[19] Y. Xu, J. Feng, T. Yu, J. Li, X. Han, H. Huang, Z. Li, Z. Zou, *ACS Appl. Energy Mater.* **2019**, *2*, 5753–5758.

[20] P. Cui, D. Wei, J. Ji, H. Huang, E. Jia, S. Dou, T. Wang, W. Wang, M. Li, *Nat. Energy* **2019**, *4*,

150–159.

[21] Q. Wang, Y. Shao, H. Xie, L. Lyu, X. Liu, Y. Gao, J. Huang, *Appl. Phys. Lett.* **2014**, *105*, 163508.

[22] D. Ma, J. Wu, M. Gao, Y. Xin, Y. Sun, T. Ma, *Chem. Eng. J.* **2017**, *313*, 1567–1576.

[23] H. Cai, B. Wang, L. Xiong, J. Bi, H. Hao, X. Yu, C. Li, J. Liu, S. Yang, *Nano Res.* **2022**, *15*, 1128–1134.

[24] J. Rodríguez-Torres, C. Gómez-Solís, L. M. Torres-Martínez, I. Juárez-Ramírez, *J. Photochem. Photobiol. A Chem.* **2017**, *332*, 208–214.

[25] B. Weng, Q. Quan, Y.-J. Xu, *J. Mater. Chem. A* **2016**, *4*, 18366–18377.

[26] K.-K. Liu, Q. Liu, D.-W. Yang, Y.-C. Liang, L.-Z. Sui, J.-Y. Wei, G.-W. Xue, W.-B. Zhao, X.-Y. Wu, L. Dong, C.-X. Shan, *Light Sci. Appl.* **2020**, *9*, 44.

[27] J. Tirado, C. Roldán-Carmona, F. A. Muñoz-Guerrero, G. Bonilla-Arboleda, M. Ralaiarisoa, G. Grancini, V. I. E. Queloz, N. Koch, M. K. Nazeeruddin, F. Jaramillo, *Appl. Surf. Sci.* **2019**, *478*, 607–614.

[28] Y. Zheng, L. Zheng, Y. Zhan, X. Lin, Q. Zheng, K. Wei, *Inorg. Chem.* **2007**, *46*, 6980–6986.

[29] H. Chen, S. Chen, X. Quan, Y. Zhang, *Environ. Sci. Technol.* **2010**, *44*, 451–455.

[30] C. Zhou, L. Shang, H. Yu, T. Bian, L. Z. Wu, C. H. Tung, T. Zhang, *Catal. Today* **2014**, *225*, 158–163.

[31] D. Ding, K. Liu, S. He, C. Gao, Y. Yin, *Nano Lett.* **2014**, *14*, 6731–6736.

[32] J. Ran, G. Gao, F. T. Li, T. Y. Ma, A. Du, S. Z. Qiao, *Nat. Commun.* **2017**, *8*, 1–10.

[33] Z. Zhang, J. T. Yates, *Chem. Rev.* **2012**, *112*, 5520–5551.

[34] S. Park, W. J. Chang, C. W. Lee, S. Park, H.-Y. Ahn, K. T. Nam, *Nat. Energy* **2016**, *2*, 16185.

[35] Z. Guan, Y. Wu, P. Wang, Q. Zhang, Z. Wang, Z. Zheng, Y. Liu, Y. Dai, M.-H. Whangbo, B. Huang,

Appl. Catal. B Environ. **2019**, *245*, 522–527.

[36] Y. Wu, P. Wang, Z. Guan, J. Liu, Z. Wang, Z. Zheng, S. Jin, Y. Dai, M.-H. Whangbo, B. Huang, *ACS Catal.* **2018**, *8*, 10349–10357.

[37] Y. Guo, G. Liu, Z. Li, Y. Lou, J. Chen, Y. Zhao, *ACS Sustain. Chem. Eng.* **2019**, *7*, 15080–15085.

[38] Y. Wu, Q. Wu, Q. Zhang, Z. Lou, K. Liu, Y. Ma, Z. Wang, Z. Zheng, H. Cheng, Y. Liu, D. Ying, B. Huang, P. Wang, *Energy Environ. Sci.* **2022,** DOI: 10.1039/d1ee03679c.

[39] X. Feng, H. Ju, T. Song, T. Fang, W. Liu, W. Huang, *ACS Sustain. Chem. Eng.* **2019**, *7*, 5152–5156.

[40] Y. Zhao, Y. Wang, X. Liang, H. Shi, C. Wang, J. Fan, X. Hu, E. Liu, *Appl. Catal. B Environ.* **2019**, *247*, 57–69.

[41] Y.-F. Xu, M.-Z. Yang, H.-Y. Chen, J.-F. Liao, X.-D. Wang, D.-B. Kuang, *ACS Appl. Energy Mater.* **2018**, *1*, 5083–5089.

[42] Y. Wu, P. Wang, X. Zhu, Q. Zhang, Z. Wang, Y. Liu, G. Zou, Y. Dai, M. H. Whangbo, B. Huang, *Adv. Mater.* **2018**, *30*, 1704342.

[43] W. Zhang, Q. Zhao, X. Wang, X. Yan, J. Xu, Z. Zeng, *Catal. Sci. Technol.* **2017**, *7*, 2753–2762.

[44] H. Huang, H. Yuan, K. P. F. Janssen, G. Solís-Fernández, Y. Wang, C. Y. X. Tan, D. Jonckheere, E. Debroye, J. Long, J. Hendrix, J. Hofkens, J. A. Steele, M. B. J. Roeffaers, *Acs Energy Lett.* **2018**, 755–759.

[45] X. Zhao, S. Chen, H. Yin, S. Jiang, K. Zhao, J. Kang, P. F. Liu, L. Jiang, Z. Zhu, D. Cui, P. Liu, X. Han, H. G. Yang, H. Zhao, *Matter* **2020**, *3*, 935–949.

[46] X.-D. Wang, Y.-H. Huang, J.-F. Liao, Y. Jiang, L. Zhou, X.-Y. Zhang, H.-Y. Chen, D.-B. Kuang, *J. Am. Chem. Soc.* **2019**, *141*, 13434–13441.

[47] H. Huang, H. Yuan, J. Zhao, G. Solís-Fernández, C. Zhou, J. W. Seo, J. Hendrix, E. Debroye, J. A.

Steele, J. Hofkens, J. Long, M. B. J. Roeffaers, *ACS Energy Lett.* **2019**, *4*, 203–208.

[48] H. Wang, X. Wang, R. Chen, H. Zhang, X. Wang, J. Wang, J. Zhang, L. Mu, K. Wu, F. Fan, X. Zong, C. Li, *ACS Energy Lett.* **2019**, *4*, 40–47.

[49] C. Wang, H. Huang, B. Weng, D. Verhaeghe, M. Keshavarz, H. Jin, B. Liu, H. Xie, Y. Ding, Y. Gao, H. Yuan, J. A. Steele, J. Hofkens, M. B. J. Roeffaers, *Appl. Catal. B Environ.* **2022**, *301*, 120760.

[50] J. Low, C. Jiang, B. Cheng, S. Wageh, A. A. Al-Ghamdi, J. Yu, *Small Methods* **2017**, *1*, 1700080.

[51] Q. Xu, L. Zhang, J. Yu, S. Wageh, A. A. Al-Ghamdi, M. Jaroniec, *Mater. Today* **2018**, *21*, 1042–1063.

[52] Y. Jiang, J. F. Liao, H. Y. Chen, H. H. Zhang, J. Y. Li, X. D. Wang, D. Bin Kuang, *Chem* **2020**, *6*, 766–780.

[53] M. Ou, W. Tu, S. Yin, W. Xing, S. Wu, H. Wang, S. Wan, Q. Zhong, R. Xu, *Angew. Chemie Int. Ed.* **2018**, *57*, 13570–13574.

[54] S. Schünemann, M. van Gastel, H. Tüysüz, *ChemSusChem* **2018**, *11*, 2057–2061.

[55] F. Xu, K. Meng, B. Cheng, S. Wang, J. Xu, J. Yu, *Nat. Commun.* **2020**, *11*, 4613.

[56] L. Canil, T. Cramer, B. Fraboni, D. Ricciarelli, D. Meggiolaro, A. Singh, M. Liu, M. Rusu, C. M. Wolff, N. Phung, Q. Wang, D. Neher, T. Unold, P. Vivo, A. Gagliardi, F. De Angelis, A. Abate, *Energy Environ. Sci.* **2021**, *14*, 1429–1438.

[57] T. Tachikawa, S. Yamashita, T. Majima, *J. Am. Chem. Soc.* **2011**, *133*, 7197–7204.

[58] E. Debroye, J. Van Loon, X. Gu, T. Franklin, J. Hofkens, K. P. F. Janssen, M. B. J. Roeffaers, *Part. & Part. Syst. Charact.* **2016**, *33*, 412–418.

[59] Z. L. Liu, R. R. Liu, Y. F. Mu, Y. X. Feng, G. X. Dong, M. Zhang, T. B. Lu, *Sol. RRL* **2021**, *5*, 1–9.

[60] Y. Jiang, H.-Y. Chen, J.-Y. Li, J.-F. Liao, H.-H. Zhang, X.-D. Wang, D.-B. Kuang, *Adv. Funct.*

Mater. **2020**, *30*, 2004293.

[61] W. Shang, Y. Li, H. Huang, F. Lai, M. B. J. Roeffaers, B. Weng, *ACS Catal.* **2021**, *11*, 4613–4632.

[62] G. Liu, J. C. Yu, G. Q. (Max) Lu, H.-M. Cheng, *Chem. Commun.* **2011**, *47*, 6763–6783.

[63] M. Wang, Y. Zuo, J. Wang, Y. Wang, X. Shen, B. Qiu, L. Cai, F. Zhou, S. P. Lau, Y. Chai, *Adv. Energy Mater.* **2019**, *9*, 1901801.

[64] Y. Zhao, Y. Dai, Q. Wang, Y. Dong, T. Song, A. Mudryi, Q. Chen, Y. Li, *ChemCatChem* **2021**, *13*, 2592–2598.

Entry for the Table of Contents

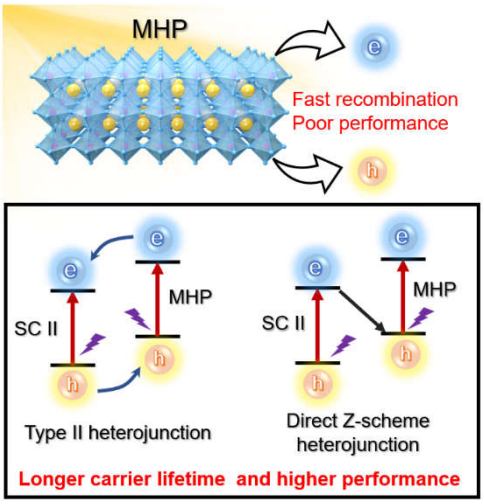

In this review, we systematically discuss the recent advances in constructing the MHP-based heterojunctions photocatalysts, including Schottky, type-II, and Z-scheme heterojunctions, with improved carriers separation and accelerated surface reaction rate for efficient solar energy conversion.